Wave front evolution of negatively refracted waves in a photonic crystal

Ethan Schonbrun,[a] Qi Wu, and Wounjhang Park
Department of Electrical and Computer Engineering, University of Colorado, Boulder, Colorado 80309

Tsuyoshi Yamashita and Christopher J. Summers
School of Material Science and Engineering, Georgia Institute of Technology, Atlanta, Georgia 30332

Maxim Abashin and Yeshaiahu Fainman
Department of Electrical and Computer Engineering, University of California, San Diego, California 92093

(Received 27 October 2006; accepted 27 December 2006; published online 25 January 2007)

Using a heterodyne near-field scanning microscope, the authors analyze the phase and amplitude of the electric field of an optical wave across the boundary of positive to negative refraction media. The photonic crystal acts as an extremely anisotropic material with a negative curvature of its dispersion surface whose shape is resolved experimentally. This extreme anisotropy results in the beam having a peculiar phase evolution through propagation that does not occur in isotropic media. A focusing wave is produced by negative refraction, which has diverging wave fronts before the internal focus and converging wave fronts after the focus. © *2007 American Institute of Physics*.
[DOI: 10.1063/1.2435344]

Waves interact strongly with periodic materials when the periodicity is on the same order as the wavelength. Materials with periodic index perturbations are critical in the field of optics, for example, in thin film mirrors, spectrally dispersive devices, and waveguide couplers. Traditionally in these devices, analysis of the transmitted or reflected wave is the most important metric in understanding their performance. The field of photonic crystals (PCs) takes a slightly different approach, where the functionality occurs while the wave is traveling through the periodic media. Currently, a few devices work with a similar approach, such as fiber Bragg gratings, distributed feedback lasers, and periodically poled nonlinear elements, but these devices employ one-dimensional periodicity. Photonic crystal devices use two and three dimensionally periodic materials, which have the capability of more complex optical properties.[1] The optical response in these materials is a strong function of frequency, polarization, and wave vector. Arising from their anomalous dispersion properties, these materials support optical effects that do not occur in natural materials such as negative refraction,[2–5] self-collimation,[6] and the superprism effect.[7] Observing waves inside the material that supports them is crucial for understanding their behavior.

When the wavelength of light is much larger than the unit cell size of a photonic crystal, the wave does not see periodic index perturbations and propagates isotropically. As the wavelength decreases, the wave starts to interact with different crystalline periodicities, which causes the dispersion curve to bend near each Bragg resonance. In a square lattice of air holes in a high index dielectric material, the first two Bragg peaks for transverse electric (TE) (*E* field in the plane of periodicity) waves are the first order interactions at the *X* point (in the ⟨10⟩ direction) and the *M* point (in the ⟨11⟩ direction). If the index contrast is large enough, the two Bragg resonances begin to overlap, opening a two-dimensional (2D) band gap. Below the Bragg resonance at the *M* point there exist frequency regions exhibiting self-collimation and negative refraction. Both of these effects arise from the directional band gap in the ⟨10⟩ direction, which induces a change in curvature of the dispersion surface in the ⟨11⟩ direction.

Figure 1 shows the dispersion surface calculated with a three-dimensional expansion of plane waves and the supercell method using the slab's finite thickness.[8] Close to the band edge, incident light sees a circular equifrequency surface (EFS) centered not at the origin, the Γ point, but at the *M* point. While the direction of the refracted *k* vector is dictated by the conservation of tangential momentum and stays at a positive angle, the direction of the energy flow, the *S* vector, is dictated by this change of curvature and reverses to a negative angle. The angle between the refracted PC *k* vector and the refracted PC *S* vector is dependent on the incident angle and can be larger than 90° close to the directional band gap. This walk-off angle resembles that of natural anisotropic crystals, but the main difference here is that the PC's EFS is circular, which means that refraction of the *S* vector is isotropic, while the refraction of the *k* vector is extremely anisotropic.

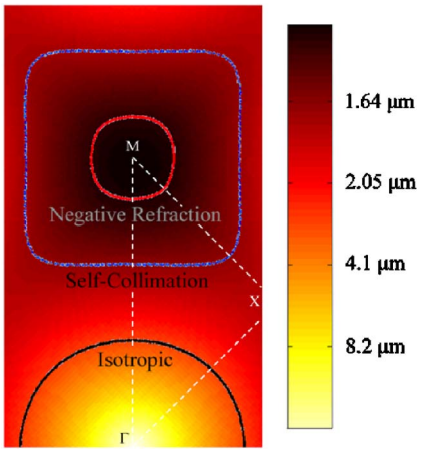

FIG. 1. (Color online) EFS for the three propagation regimes in the first band. The dispersion diagram is evaluated for a TE-like mode in a square PC with a period of 410 nm and a hole diameter of 295 nm in a 300 nm film of silicon.

[a]Electronic mail: schonbru@colorado.edu

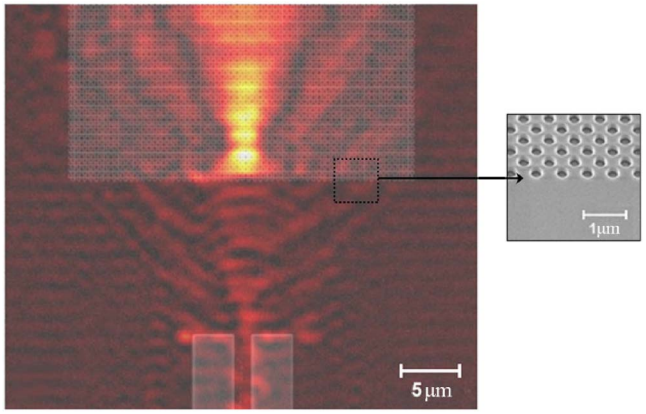

FIG. 2. (Color online) Field amplitude as measured by a heterodyne NSOM with a low resolution scan. The sample is illuminated with 1560 nm light in the TE polarization. The inset shows a scanning electron micrograph of the positive to negative refraction interface. The positive index material consists of an unpatterned region of silicon. The negative refraction material is the same as that modeled in Fig. 1.

Based on the analysis of Fig. 1, we designed and fabricated a negatively refracting photonic crystal structure on a 300 nm thick silicon-on-insulator (SOI) substrate. Figure 2 shows the guided wave amplitude in three different stages of the device as measured by the scanning near-field optical microscope (NSOM). First, light propagates through a 2 μm wide ridge waveguide, where it has a fundamental mode width of 1.5 μm. The mode then diffracts across a 15 μm long region of unpatterned SOI substrate expanding to a width of 6.6 μm. Finally, the beam refracts across the PC interface, which is a square lattice of holes orientated in the $\langle 11 \rangle$ direction. The Bloch mode excited in the PC negatively refracts and forms an internal focus 3 μm behind the interface, which has a beam waist size of 2.6 μm. Beyond the internal focus, the beam continues to expand through the PC.

Analysis of the field amplitude gives the profile of the wave, but misses the phase behavior that occurs at the positive to negative refraction interface and internal focus. In order to retrieve the full complex field of the guided wave, we make heterodyne interferometric measurements with the NSOM.[9–11] The signal detected by the near-field probe is coherently mixed with a frequency-shifted version of the laser signal and fed to a lock-in amplifier, where both the amplitude and phase are evaluated.[12] In order to resolve the details of the phase, the field is imaged under high resolution where the spatial samples have a period of 110 nm, which give four to five measurements per cycle.

Under high resolution, several interesting features are visible in the detected NSOM image shown in Figs. 3(a) and 3(b). The geometry of the PC appears in both amplitude, Fig. 3(a), and phase, Fig. 3(b), scans, showing that the wave in the crystal is a strongly modulated Bloch wave. Yet in this case, the phase fronts of the wave resemble those of a plane wave because only the first photonic band is excited. More interesting is that we can resolve the curvature of the wave fronts in the phase image both across the interface and into the PC. Unlike a normal focusing wave, the phase fronts are not converging and, on traversing across the interface from the silicon to the PC, their curvature does not change sign. The sign of the curvature does change at the internal focus where the wave fronts change from diverging to converging. The curvature of the wave fronts may be seen more clearly in

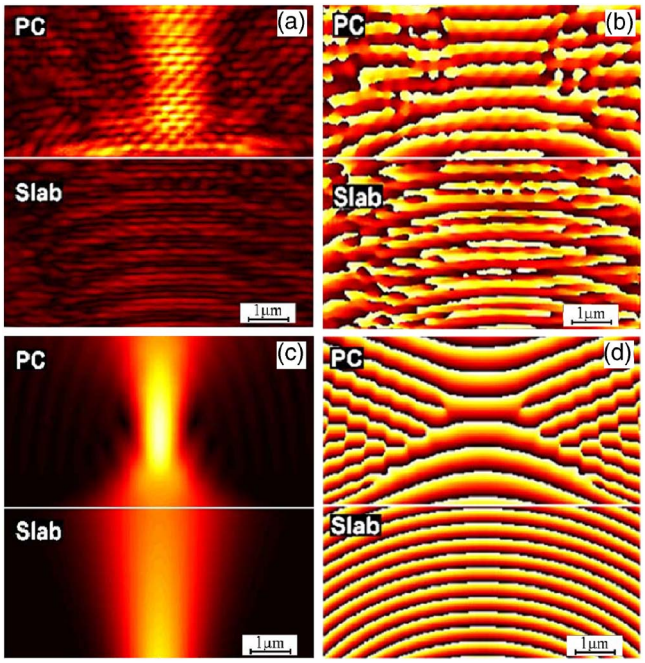

FIG. 3. (Color online) Amplitude, evaluated experimentally in (a) and numerically in (c), and the phase, evaluated experimentally in (b) and numerically in (d), of the field at the slab/PC interface, where the wave travels from bottom to top. The collection efficiency of the NSOM probe is larger over the PC region because the wave has smaller in-plane confinement than in the slab.

the numerical simulation shown in Fig. 3(d). Wave propagation is modeled with a split step Fourier beam propagation method to calculate the complex field, using the transfer function,

$$H(\nu_x) = e^{j(\sqrt{(k_0 n_m)^2 - (2\pi\nu_x)^2} + \sqrt{2}\pi/a)dz}, \quad (1)$$

where n_m is the index inside the PC calculated from the radius of the EFS, $\sqrt{2}\pi/a$ is the origin of the circular EFS centered at the M point, k_0 is the wave vector in air, and ν_x is the spatial frequency in the transverse plane. This method accurately models the anisotropic EFS but ignores the periodicity of the crystal.

Analysis of the complex field allows us also to look at the spatial frequency components in Fourier space for both the silicon slab and the PC. Fourier analysis has been used recently to numerically analyze finite-difference time-domain (FDTD) simulation data in PCs to better understand the spectrum of momentum inside a crystal.[13] In this letter, we compare the 2D Fourier transform of the complex field data numerically calculated by the FDTD method and experimentally obtained by the heterodyne NSOM, as shown in Fig. 4. The convex curvature of the PC EFS is resolved, compared to the concave shape of the silicon light line. The PC EFS is repeated at each M point in reciprocal space, but most of the energy is carried in the central order, experimentally estimated to have eight times more power than each of the other M points. The radius of curvature can also be resolved and is similar to that of an isotropic material with an index of 0.42. This value translates into a diffraction parameter that is more than twice that of air, where the diffraction parameter is defined as $1/(k_{PC} - k_m)$, where k_{PC} is the momentum vector of the Bloch wave and k_m is the reciprocal lattice vector at the M point.

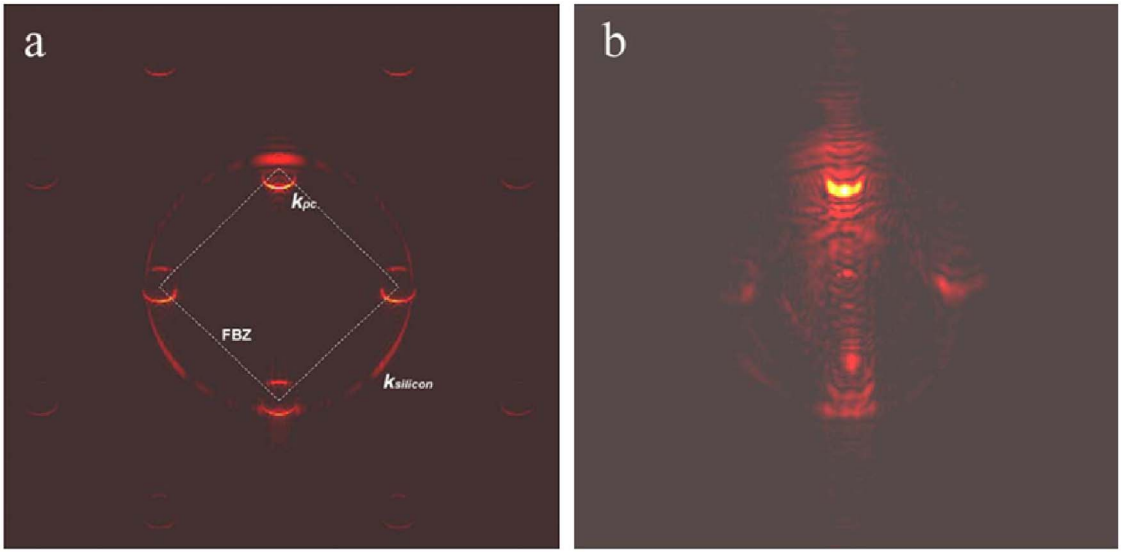

FIG. 4. (Color online) Numerical and experimental Fourier spectra of the guided light. (a) shows the Fourier transform of the complex field obtained from the FDTD data of a silicon slab to PC interface. FBZ is an outline of the first Brillioun zone, k_{silicon} is the momentum surface of the fundamental TE mode, and k_{PC} is the momentum surface of the Bloch mode. (b) shows the same for the data obtained by the NSOM.

In addition to resolving the shape of the EFS, the spectrum also allows us to calculate effective phase velocities of the Bloch mode and silicon light line. From the spectrum, the effective index of the silicon is 3.02, which is very close to the value calculated with a three-dimensional vector mode solver. The effective index of the optical axis point of the negative refraction mode is experimentally determined to be 1.83, compared to what is calculated with the FDTD method and plane wave expansion, which is 2.21. The discrepancy is close to the error margin in our Fourier analysis judging from the fact that only seven spatial cycles of the wave have been measured, and the accuracy is good to one part in five. There is also a smaller circle centered at the origin in Fig. 4(b) that is absent in Fig. 4(a). The size of this circle matches well to the second TE-like mode, which lies just above cutoff at an effective index of 1.6 and is not predicted by the 2D numerical model.

In summary, we have presented a quantitative near-field investigation on wave propagation in a negatively refracting PC structure. Direct observation of in-plane wave propagation showed internal focusing due to negative refraction. Furthermore, the complex field showed that the focusing wave fronts exhibited anomalous curvature. Anomalous wave front curvature is due to an EFS that has anomalous curvature, which was confirmed experimentally by Fourier analysis of the measured field amplitude and phase. We believe that the ability to observe and quantify the exotic dispersion properties of engineered materials is an important step in order to take full advantage of their properties.

This work was supported in part by the National Science Foundation (DMI-0304650) and by the U.S. Army Research Office under MURI Contract Nos. DAAD19-01-1-0603 and W91NF-06-1-0377.

[1]R. Zengerle, J. Mod. Opt. **34**, 1589 (1987).
[2]M. Notomi, Phys. Rev. B **62**, 10696 (2000).
[3]C. Luo, S. G. Johnson, J. D. Joannopoulos, and J. B. Pendry, Phys. Rev. B **68**, 045115 (2003).
[4]A. Berrier, M. Mulot, M. Swillo, M. Qiu, L. Thylen, A. Talneau, and S. Anand, Phys. Rev. Lett. **93**, 073902 (2004).
[5]E. Schonbrun, T. Yamashita, W. Park, and C. J. Summers, Phys. Rev. B **73**, 195117 (2006).
[6]H. Kosaka, T. Kawashima, A. Tomita, M. Notomi, T. Tamamura, T. Sato, and S. Kawakami, Appl. Phys. Lett. **74**, 1212 (1999).
[7]S. Lin, V. M. Hietala, Li Wang, and E. D. Jones, Opt. Lett. **21**, 1771 (1996).
[8]S. G. Johnson and J. D. Joannopoulos, Opt. Express **8**, 173 (2001).
[9]A. Lewis, M. Isaacson, A. Harootunian, and A. Murray, Ultramicroscopy **13**, 227 (1984).
[10]M. L. M. Balisteri, J. P. Korterik, L. Kuipers, and N. F. van Hulst, Phys. Rev. Lett. **85**, 294 (2000).
[11]P. Tortora, M. Abashin, I. Märki, W. Nakagawa, L. Vaccaro, M. Salt, H. P. Herzig, U. Levy, and Y. Fainman, Opt. Lett. **30**, 2885 (2005).
[12]A. Nesci and Y. Fainman, Proc. SPIE **5181**, 62 (2003).
[13]I. De Leon and F. S. Roux, Phys. Rev. B **71**, 235105 (2005).